Supporting Information

High-performance Na-storage cathode enabled by layered P2-type K_xMnO_2 with enlarged interlayer spacing and fast diffusion channels for sodium-ion batteries†

Ningbo Liu[a,+], Xiaoying Zhao[a,+], Bin Qin[b], Dongdong Zhao[a], Huanhuan Dong[c], Mande Qiu[a,*], and Liubin Wang[a,c,*]

[a]*College of Chemistry & Environmental Science, Key Laboratory of Medicinal Chemistry and Molecular Diagnosis (Ministry of Education), Hebei University, Baoding 071002, China*

[b]*Department of Chemistry, The University of Hong Kong, Pokfulam Road, Hong Kong SAR, China*

[c]*Key Laboratory of Advanced Energy Materials Chemistry (Ministry of Education), Nankai University, Tianjin 300071, China*

[+]These authors contributed to this work equally.
[*]Corresponding author.
E-mail address: lbwang@hbu.edu.cn (L. Wang); hbuqmd@sina.cn (M. Qiu).

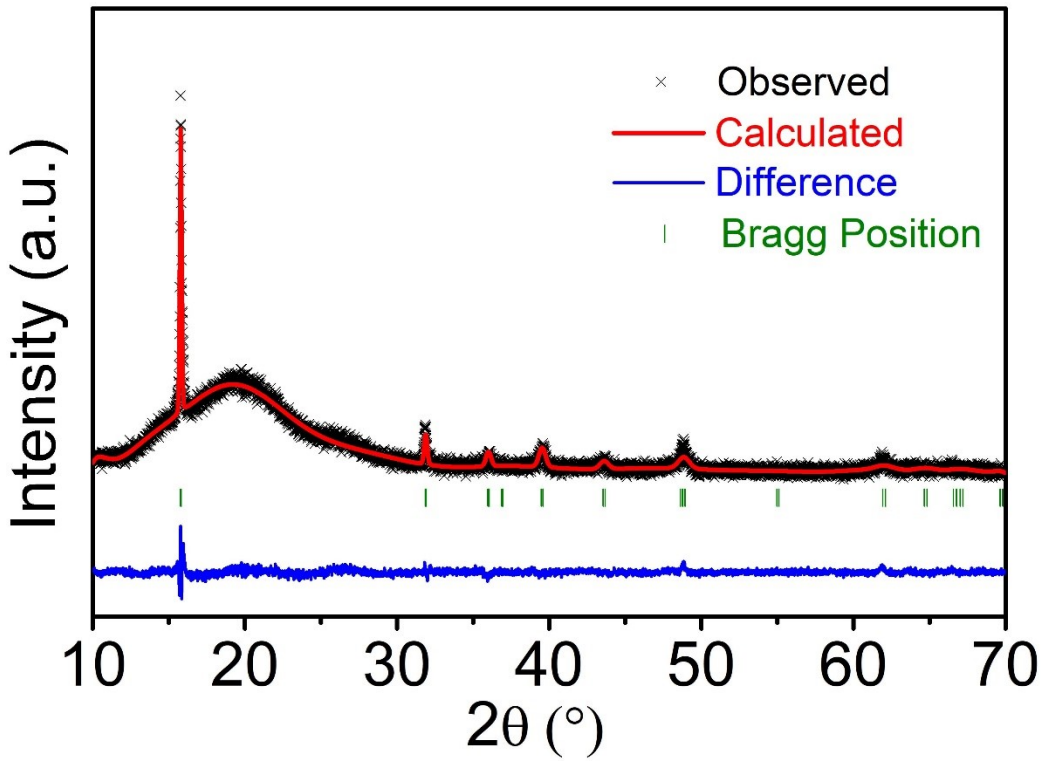

Fig. S1. Rietveld-refined XRD profile of the as-prepared NMO.

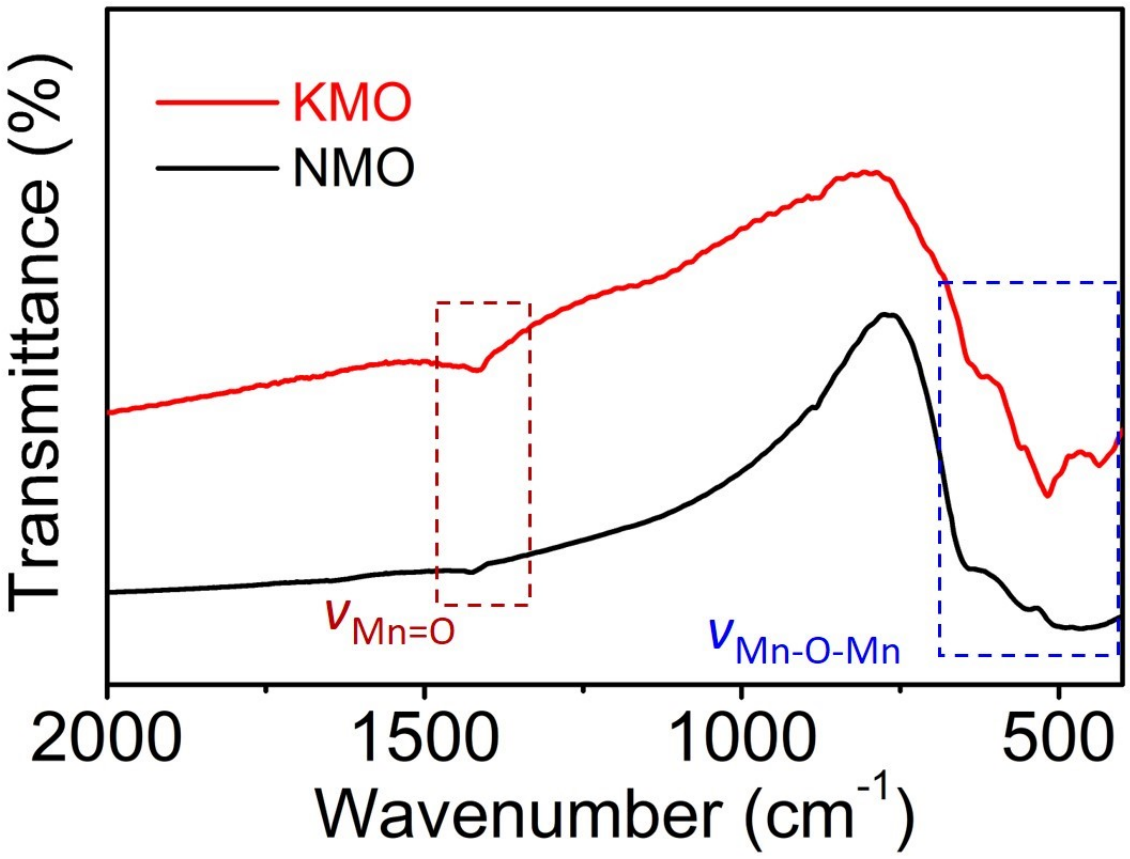

Fig. S2. FTIR spectra of the prepared KMO and NMO samples.

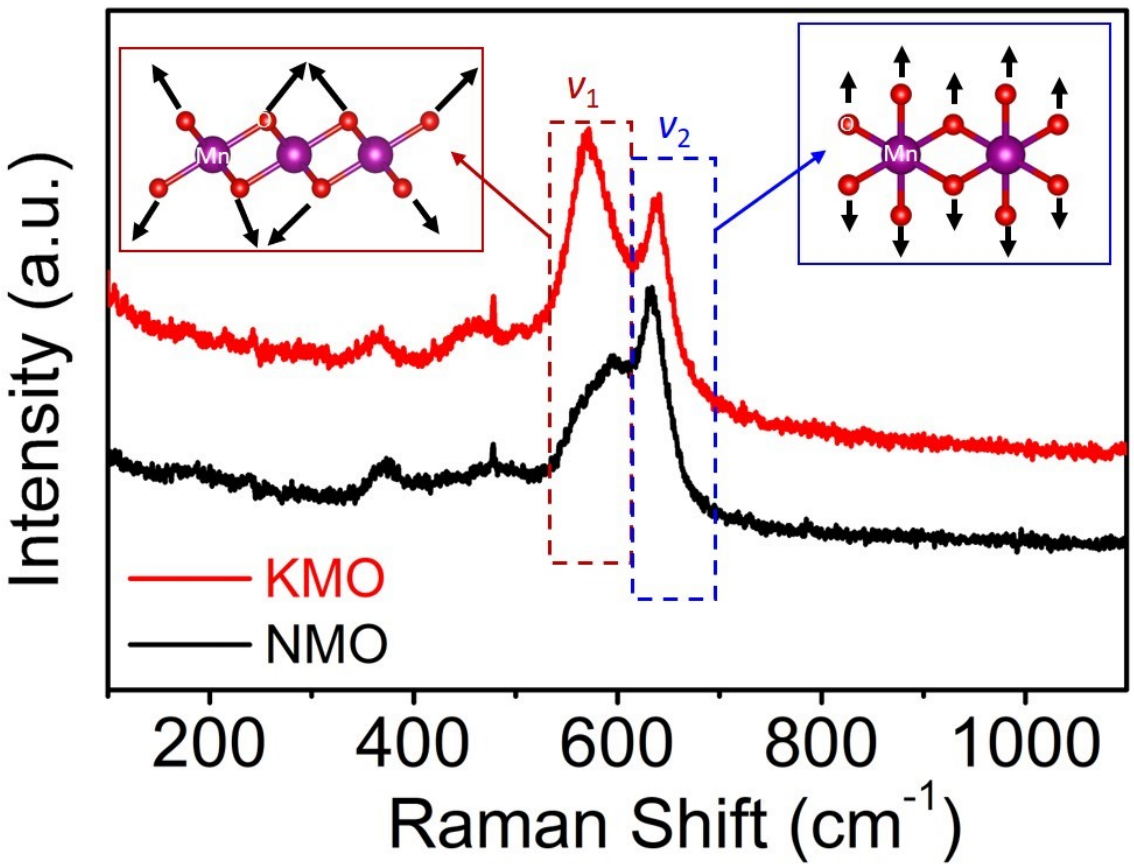

Fig. S3. Raman spectra of the prepared KMO and NMO samples.

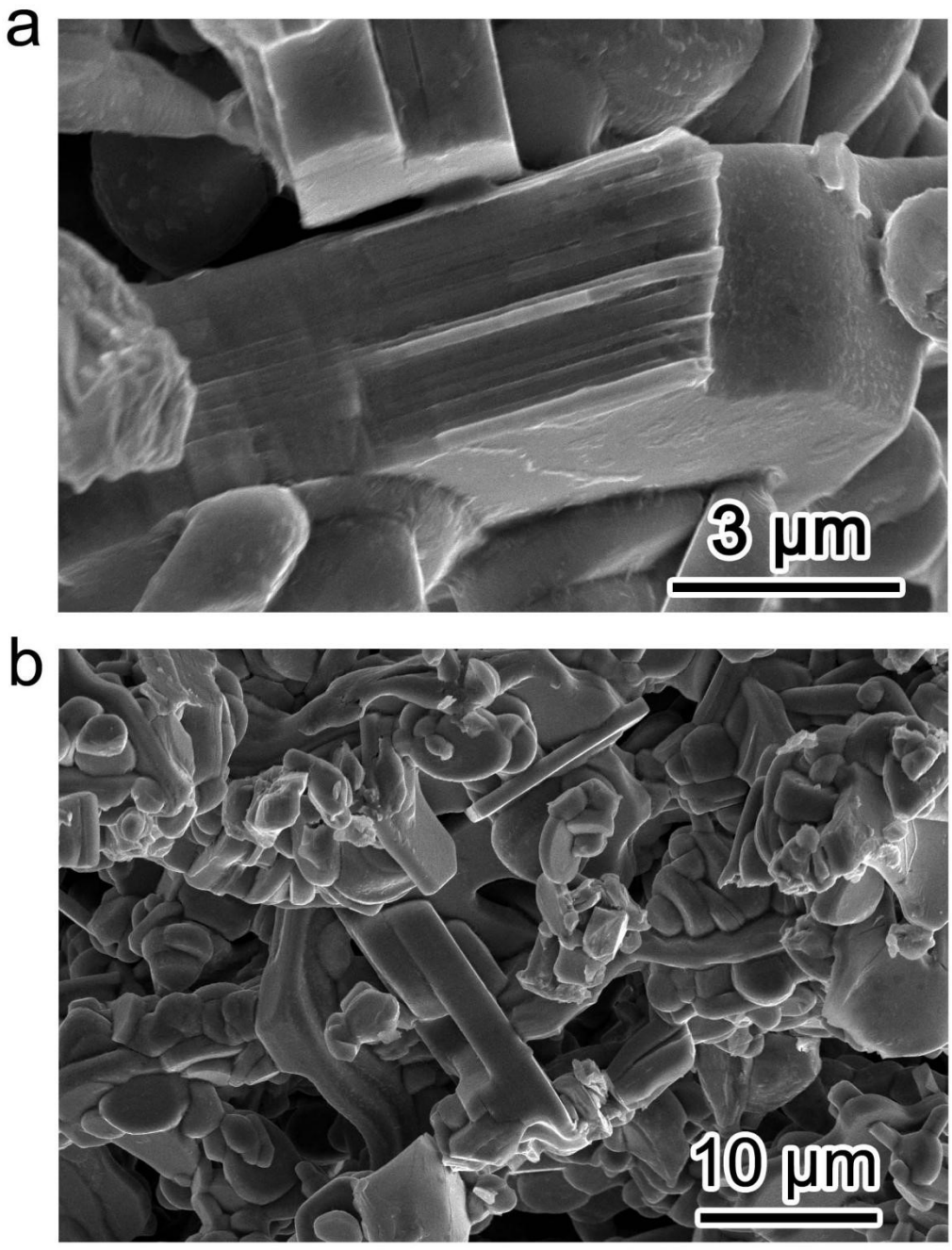

Fig. S4. SEM images of the prepared NMO samples.

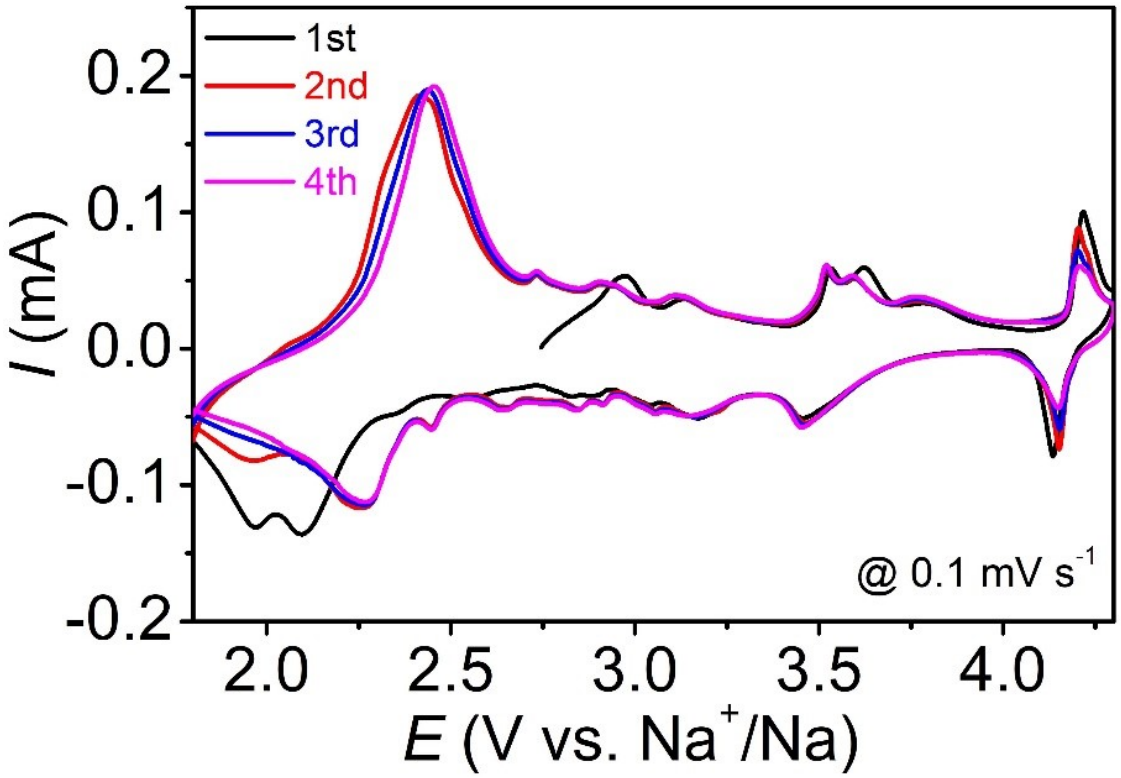

Fig. S5. CV curves of NMO electrode at 0.1 mV s^{-1} between 1.8 and 4.3 V

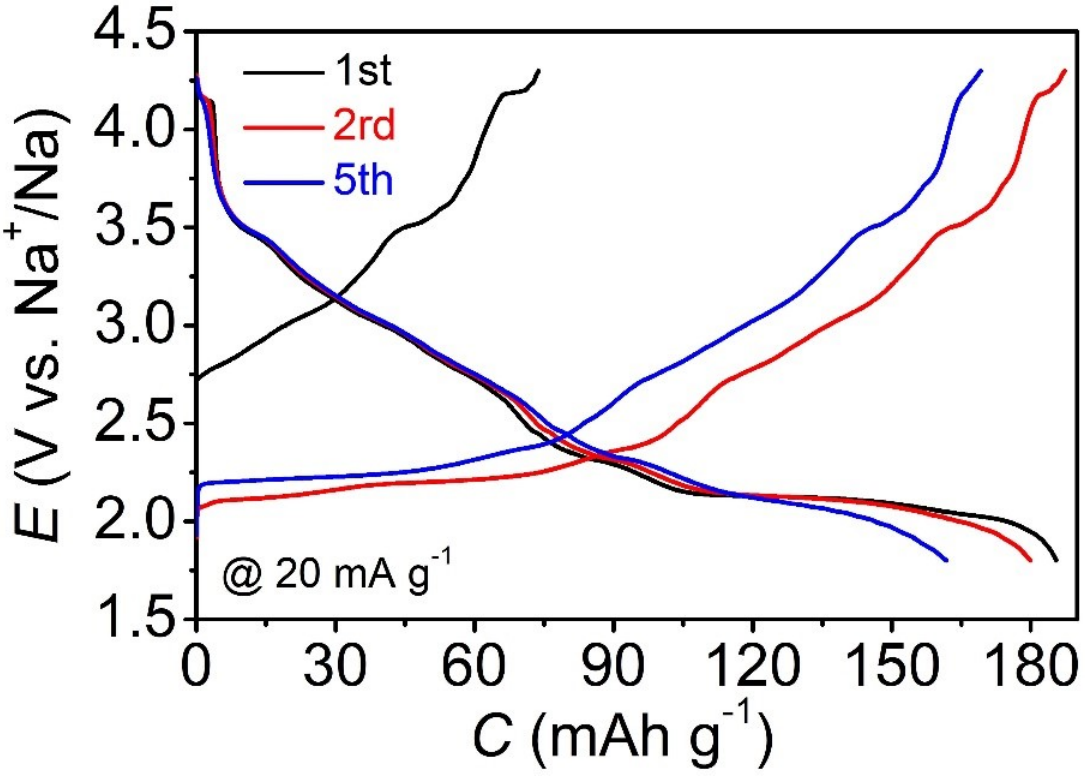

Fig. S6. Charge/discharge curves of NMO electrode at 20 mA g^{-1}.

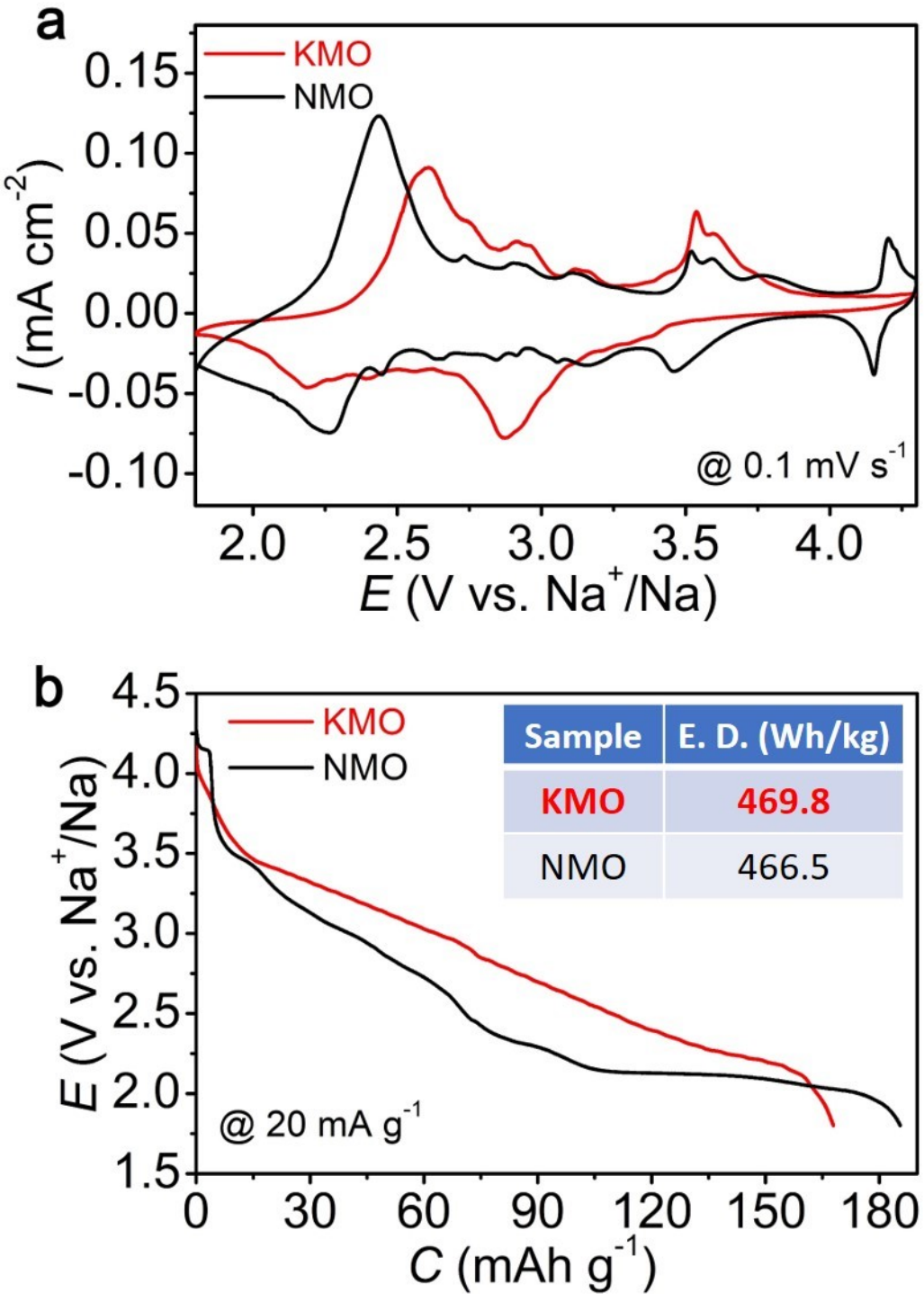

Fig. S7. Comparing the CV and charge/discharge curves of NMO and KMO electrodes.

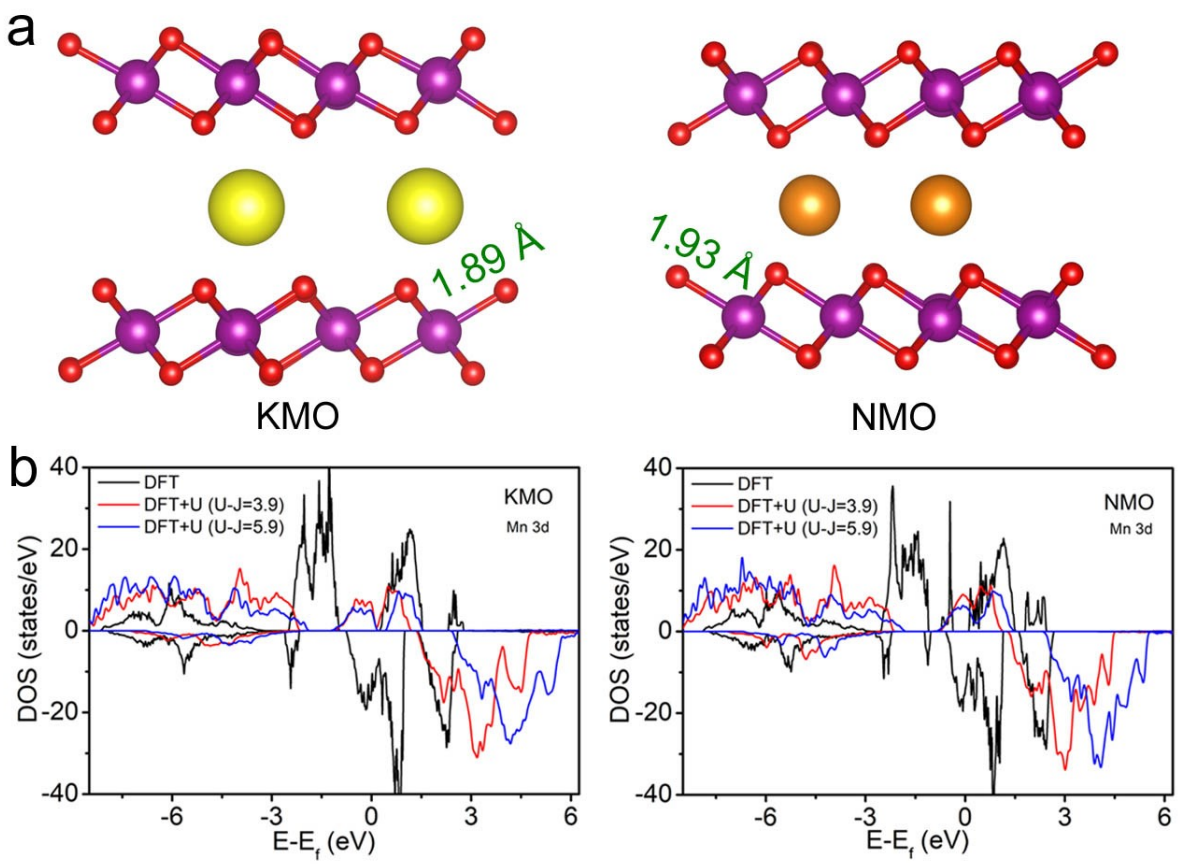

Fig. S8. (a) The bond lengths Mn-O bonds in [MnO_6] and (b) the calculated projected density of states (DOS) in the d orbitals of Mn atoms of KMO and NMO.

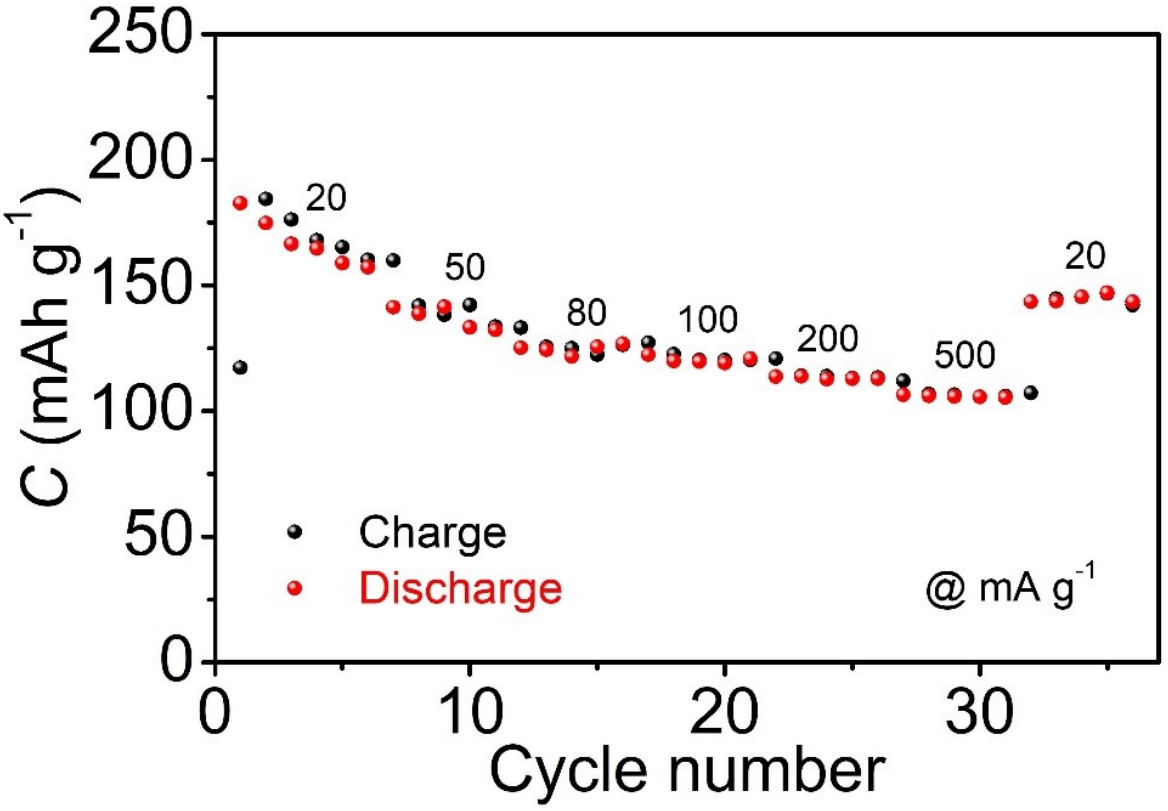

Fig. S9. Rate performance of NMO at a current density range of 20-500 mA g^{-1}.

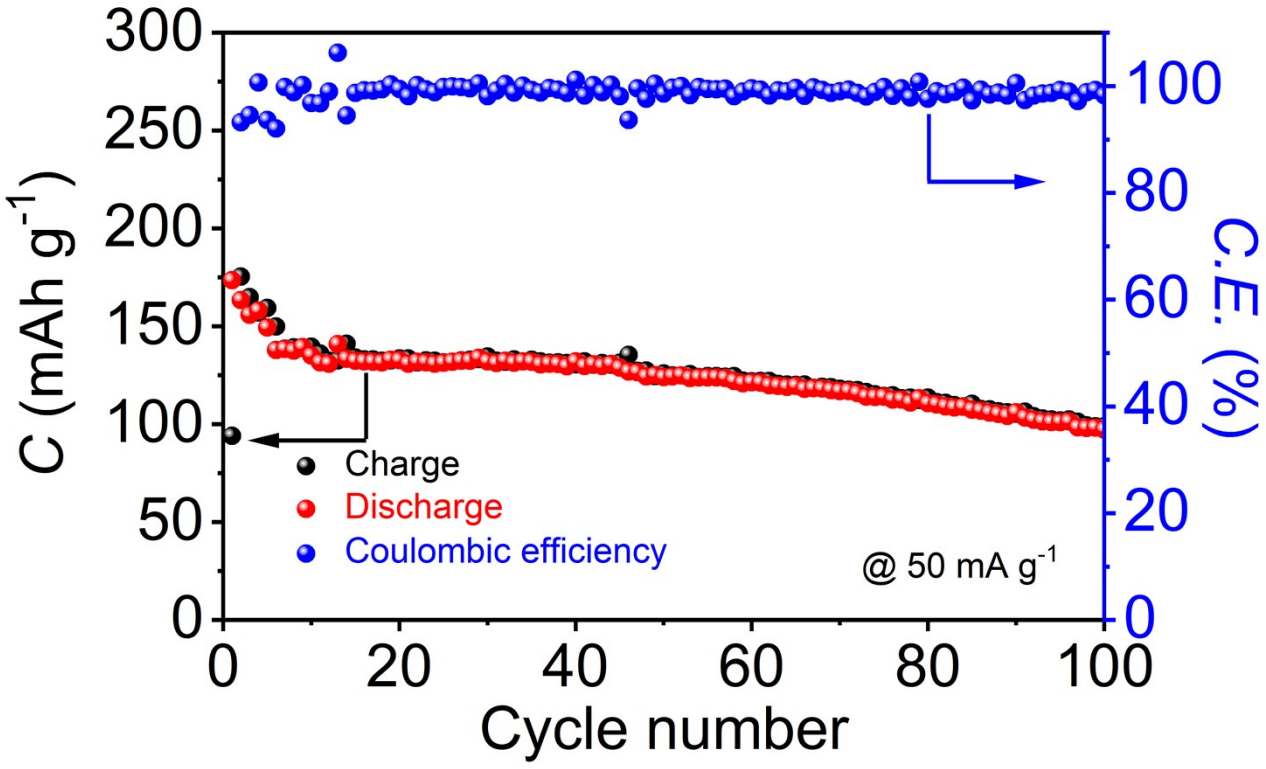

Fig. S10. Long-cycling performance of NMO at 50 mA g^{-1}.

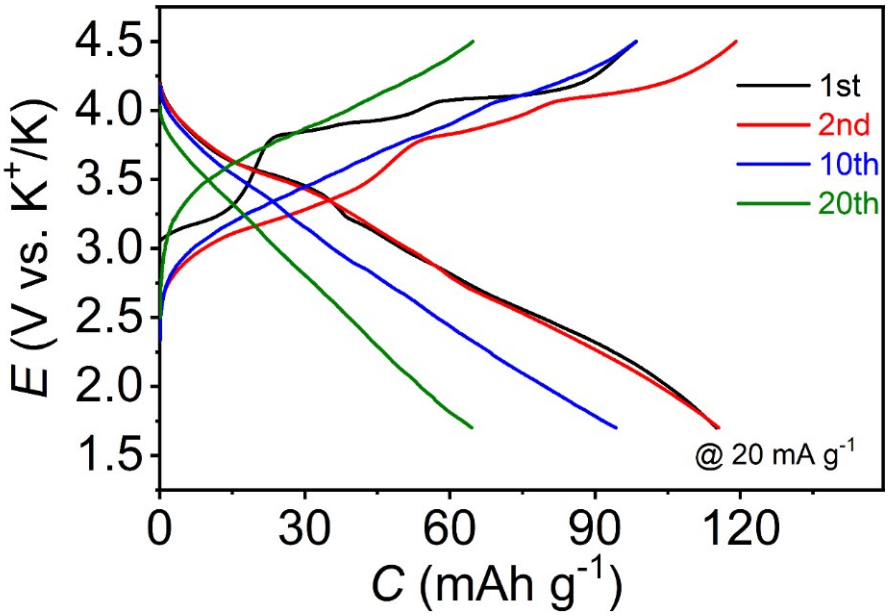

Fig. S11. Charge/discharge curves of KMO electrode in K-ion battery at 20 mA g^{-1}.

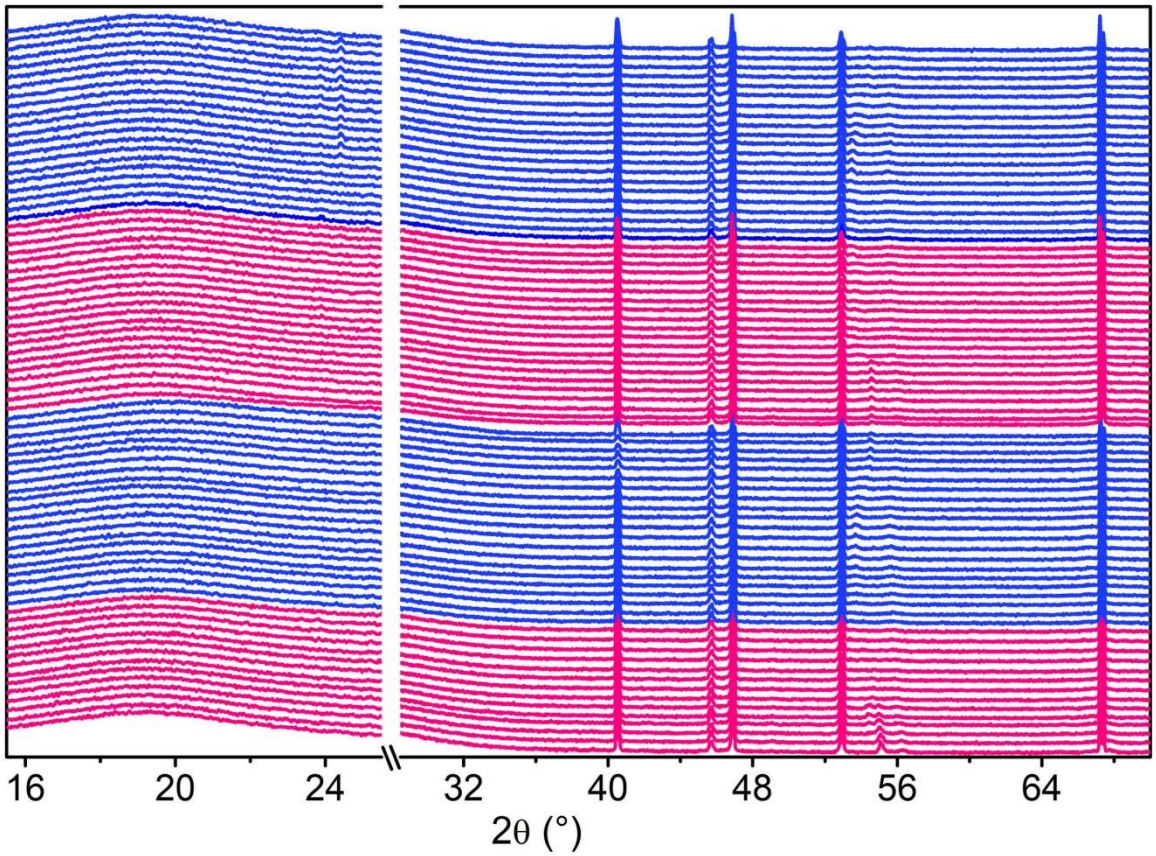

Fig. S12. In-situ XRD patterns of KMO electrode during the first two cycles.

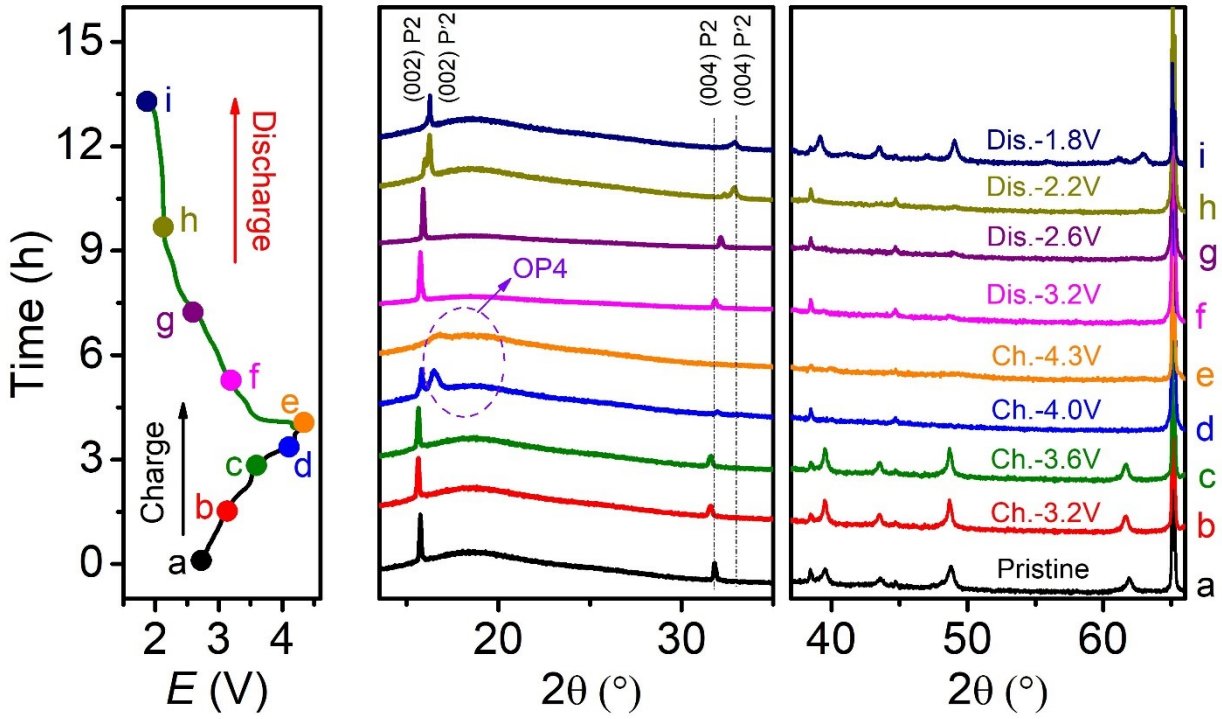

Fig. S13. Ex-situ XRD patterns of NMO during the first charge/discharge process.

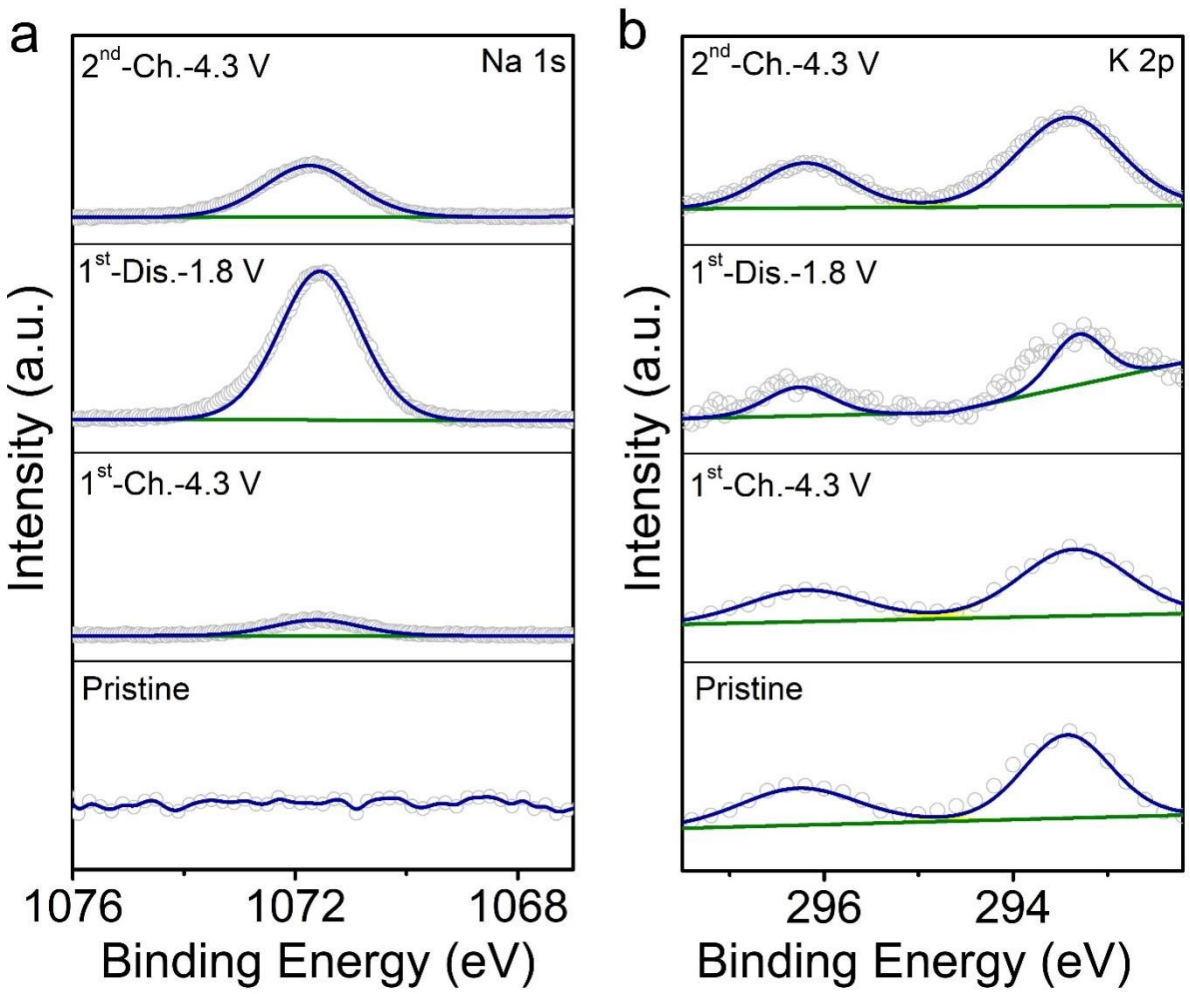

Fig. S14. XPS spectra of Na 1s and K 2p for the KMO electrode at different charge/discharge states.

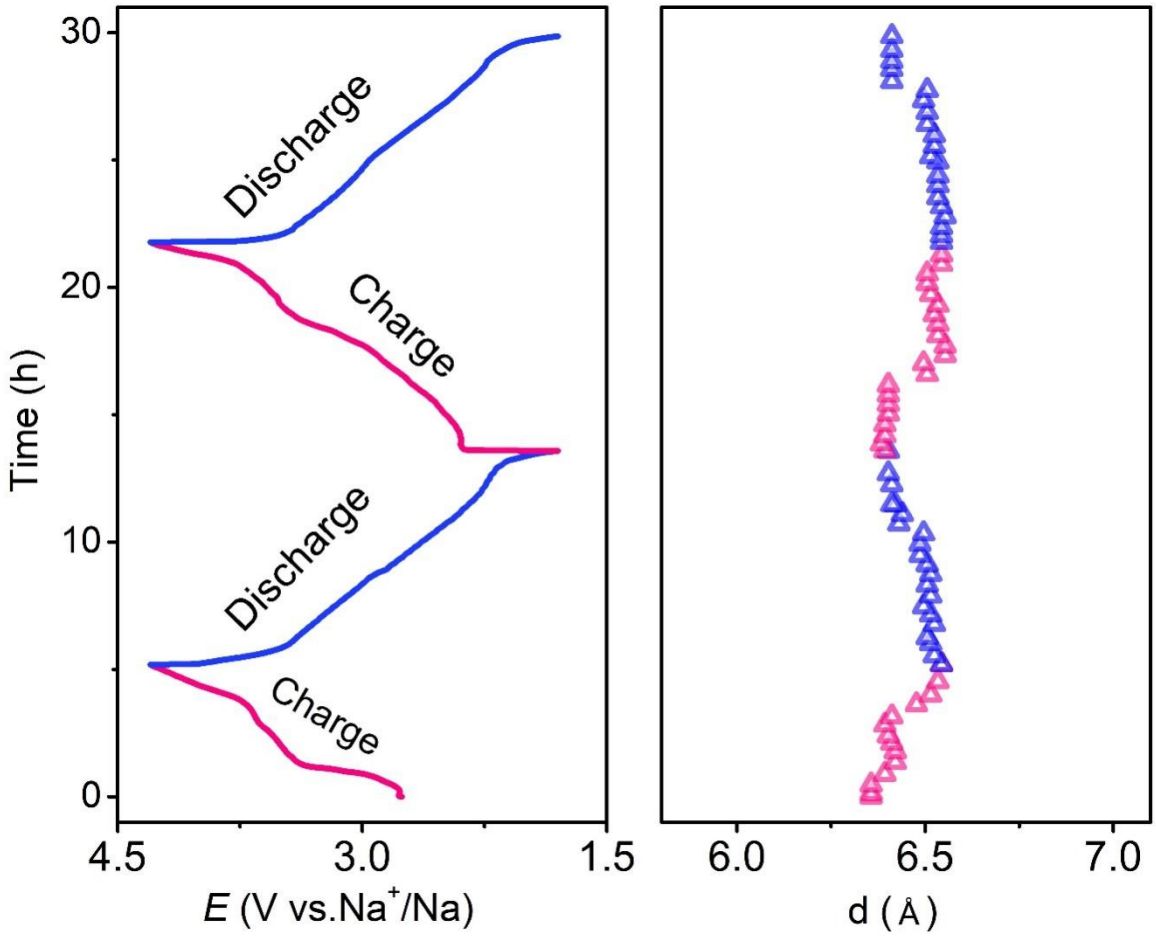

Fig. S15. The variation of the interlayer spacing of (002) facets along with Na^+ extraction and insertion for KMO.

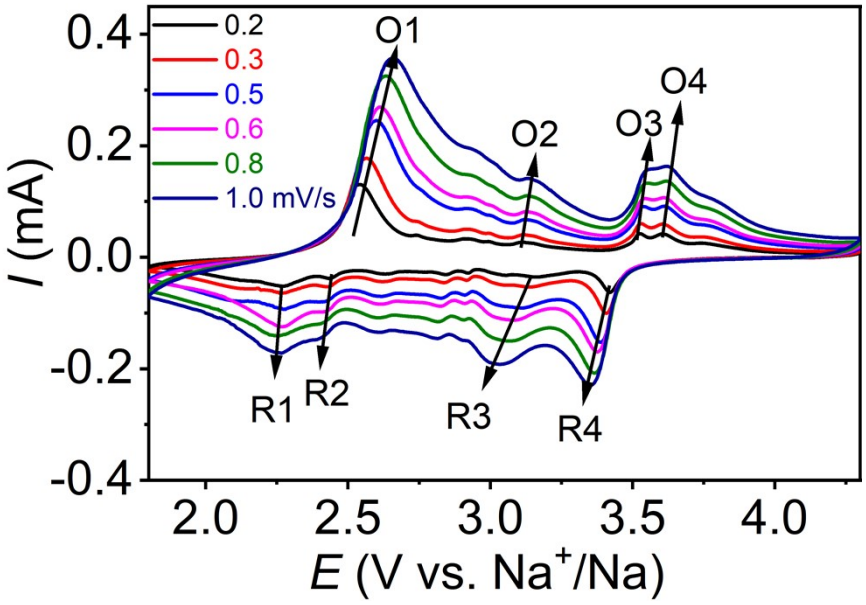

Fig. S16. CV curves of NMO electrode at different scan rates from 0.2 to 1.0 mV s^{-1}.

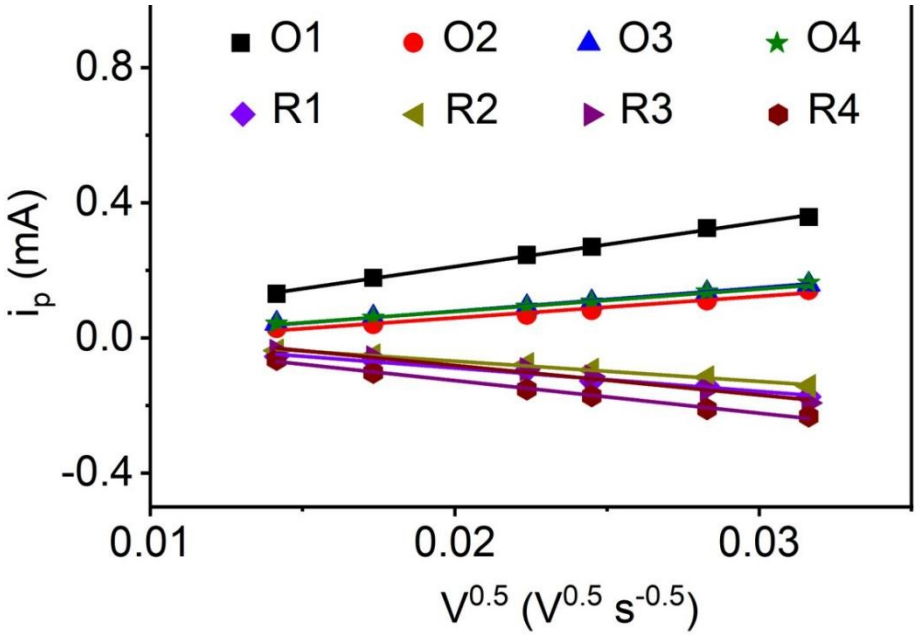

NMO	O1	O2	O3	O4
D_{Na+} (cm^2 s^{-1})	1.14×10^{-10}	2.71×10^{-11}	2.92×10^{-11}	3.22×10^{-11}
	R1	R2	R3	R4
D_{Na+} (cm^2 s^{-1})	3.20×10^{-11}	2.39×10^{-11}	5.10×10^{-11}	6.20×10^{-11}

Fig. S17. Corresponding fitting lines between peak current (i_p) and the square root of scan rates ($v^{0.5}$) and the calculated diffusion coefficients (D_{Na+}) at different states.

As shown in FigureS16, the peak currents (i_p) show a linear relationship with the square root of scan rates (v) as the increas of v. The diffusion coefficients of Na^+ in the NMO electrode can be calculated based on the Randles-Sevcik equation,[1] as shown below:

$$i_p = (2.69*10^5)n^{3/2}AD_{Na+}^{1/2}C_{Na+}v^{1/2} \quad \text{(S1)}$$

Where i_p (A) is the peak current, n is the number of transferred electrons per molecule (n = 0.69), A (cm^2) is the contacting area (0.785 cm^2) between electrode and electrolyte, C_{Na+} is the Na ions concentration in the electrode ($\approx 9.2 \times 10^{-3}$ mol cm^{-3}), and v (V s^{-1}) is the scan rate.

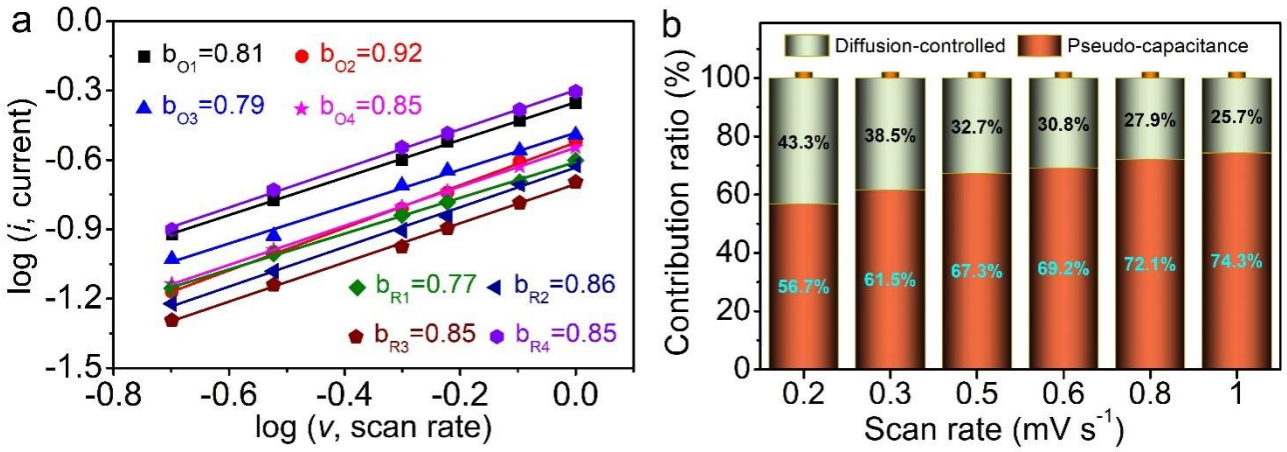

Fig. S18. (a) Corresponding log *i* vs. log *v* plots and (b) percentages of the pseudo-capacitance and diffusion-controlled reactions of KMO electrode at different scan rates.

The relationship between peak currents (*i*) and scan rates (*v*) can be described by equation $i = av^b$, where a and b refer to variable parameters. It is well-documented that b=1 and 0.5 represent a pseudo-capacitance and diffusion-controlled reactions, respectively. The b values of KMO for peaks O1, O2, O3, O4, R1, R2, R3 and R4 are 0.81, 0.92, 0.79, 085, 0.77, 0.86, 0.85 and 0.85 (Figure S17a). This indicates a mixed process controlled by both capacitive and diffusion effect of KMO electrode, rending a fast reaction kinetics. Furthermore, the pseudo-capacitive contribution can be evaluated based on the equation of $i = k_1v + k_2v^{0.5}$, where $k_1\upsilon$ and $k_2\upsilon^{0.5}$ represent the pseudocapacitive and diffusion contribution, respectively.[2] The pseudocapacitive contributions at different scan rates can be quantified and are shown in Figure S17b. The capacitive effect gradually strengthens with the scan rate increasing, and the

pseudocapacitive domination may be partially responsible for the good electrochemical performance of the KMO electrode.

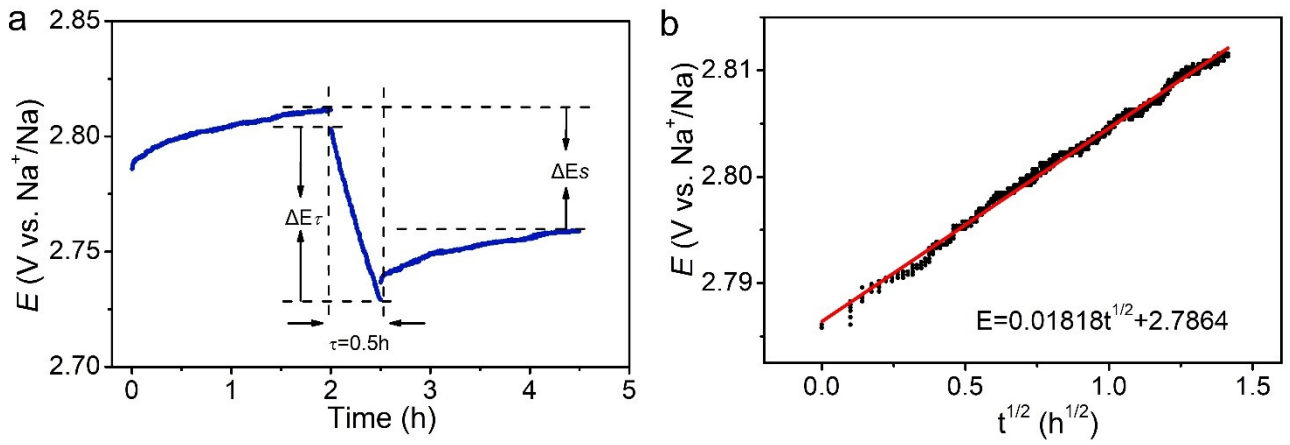

Fig. S19. (a) Current step diagram of the GITT curves and (b) linear fit of the cell potential vs. the square root of time ($\tau^{1/2}$) with different pulse currents.

The diffusion coefficient (D_{Na+}) can be calculated by Fick's law from the following equation:

$$D_{Na^+}=4/\pi\tau(m_B V_M/M_B S)^2(\Delta E_s/\Delta E_\tau)^2 \quad (S2)$$

Where D_{Na+} ($cm^2\ s^{-1}$) means the chemical diffusion coefficient, τ (s) represents the testing time in each step, V_M ($cm^3\ mol^{-1}$), m_B, and M_B are the molar volume, weight, and molar weight of the active materials, respectively, while S is the surface area of the electrode (0.785 cm^2) and ΔE_s and ΔE_τ are the quasi-equilibrium potential and the change of cell voltage E during the current pulse, respectively.[3] As indicated in Figure S18b, the cell voltage as a function of $\tau^{1/2}$ shows a linear relationship, and therefore, D_{Na+} is a function of cell voltage.

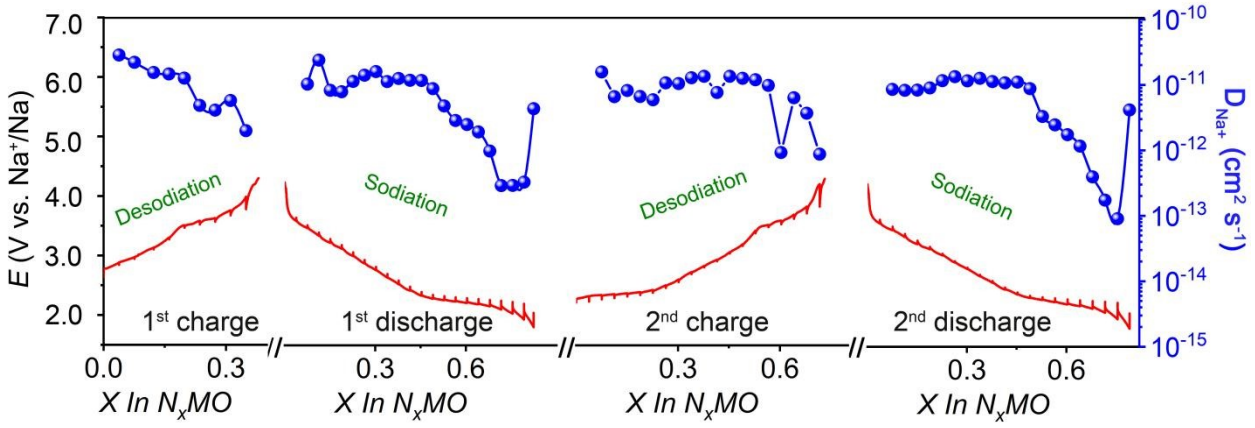

Fig. S20. GITT curves of NMO electrode in the first two cycles and the corresponding calculated diffusion coefficients.

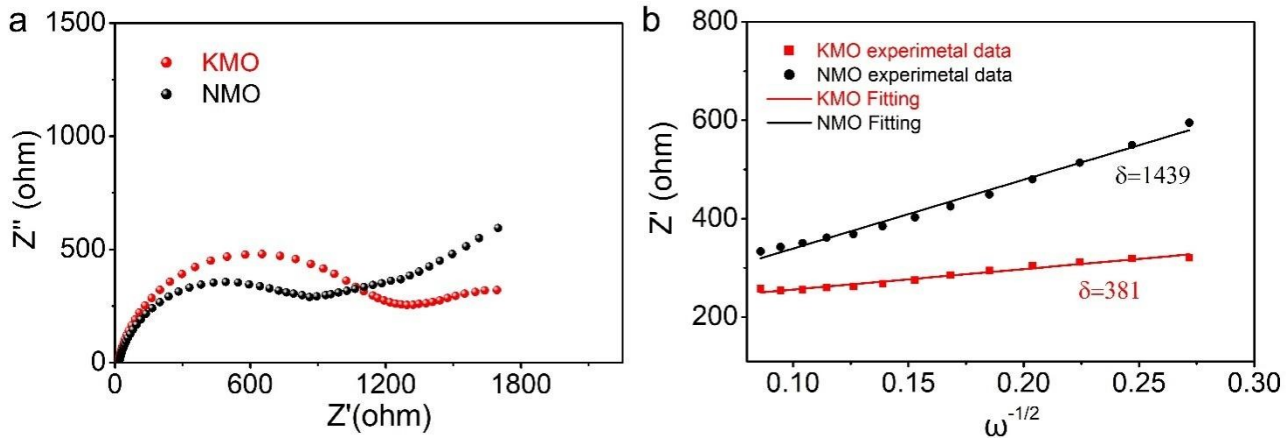

Fig. S21. (a) EIS spectra of KMO and NMO electrodes at open-circuit voltage before test; (b) the relationship between Z' and $\omega^{-1/2}$ in the low-frequency of EIS.

The Na^+ diffusion coefficients can be calculated by the formula as following:

$$D_{Na+} = R^2T^2/2A^2n^4F^4C^2\delta^2 \qquad (S3)$$

Where R is the gas constant (8.314 J K^{-1} mol^{-1}), T is the room temperature in our experiment (298 K), A is the surface area of the electrode (0.785 cm^2), n is the number of electrons per molecule attending the electronic transfer reaction, F is the Faraday constant (96500 C mol^{-1}), C is the concentration of Na^+ in electrode, σ is the slope of the line $\omega^{-1/2}$-Z', respectively. The slope of $\omega^{-1/2}$-Z' plot of KMO is smaller than that of NMO in Figure S20b, reflecting the higher Na^+ diffusion coefficients in the KMO electrode.

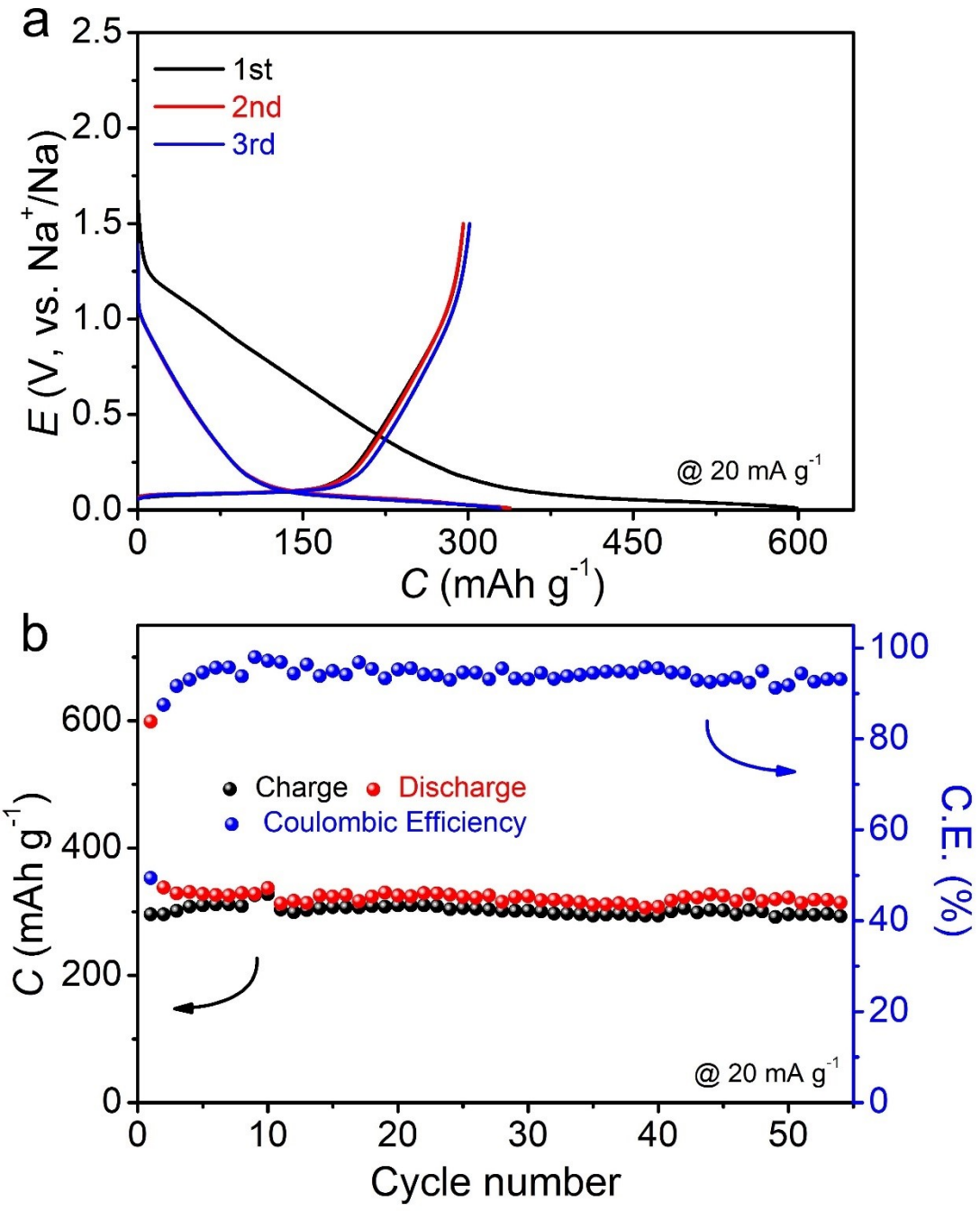

Fig. S22. Charge/discharge curves and cycling performance of HC//Na half cell.

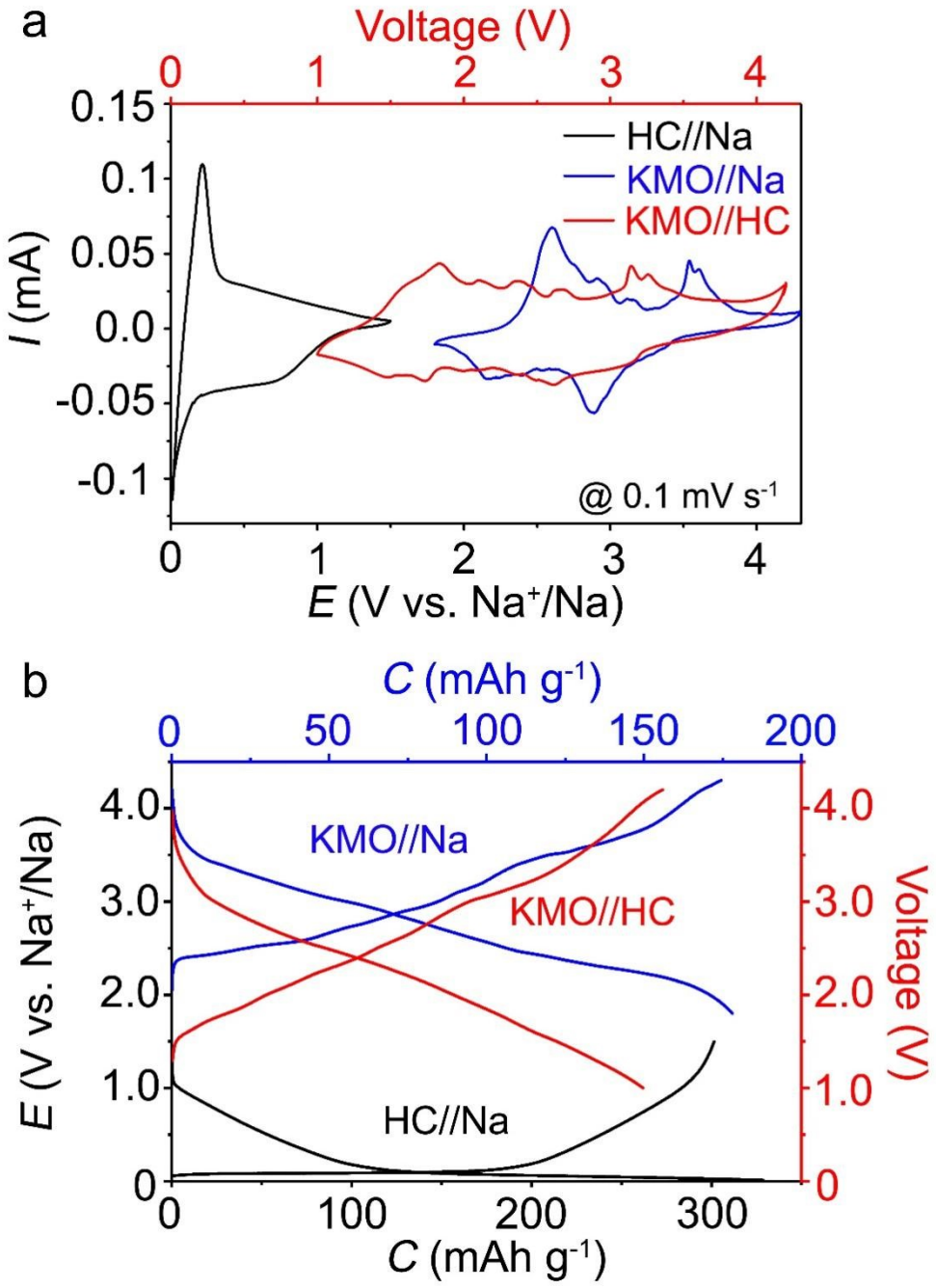

Fig. S23. Charge/discharge profiles of KMO//Na, HC//Na half cells, and KMO//HC full cells.

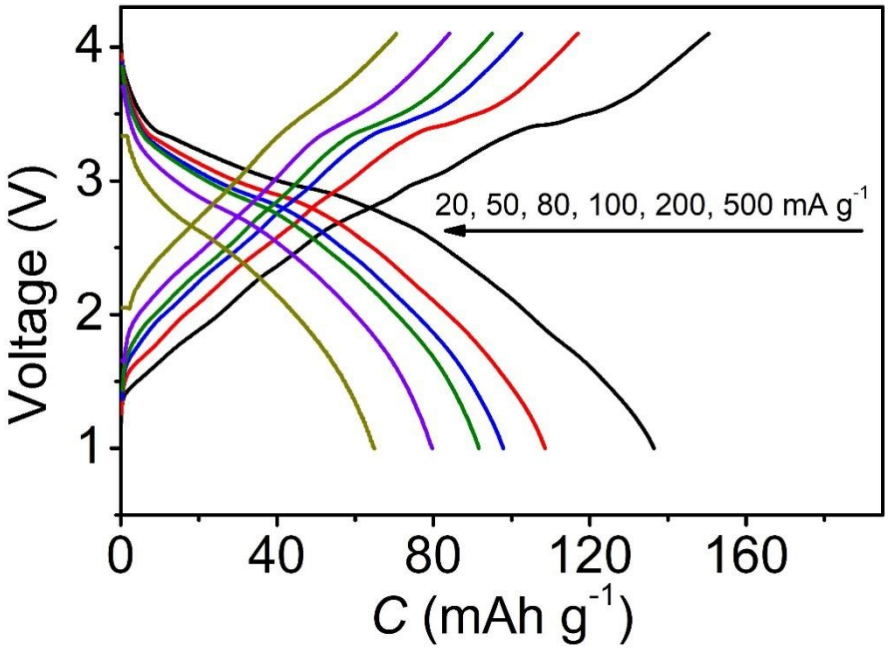

Fig. S24. Rate performance of KMO//HC full battery at different rates.

Table S1. Structural parameters and atomic position of KMO from the Rietveld refinement.

Crystal System: hexagonal**, Space Group:** P63/mmc

a = b = 2.8795 Å, c = 12.7714 Å, $\alpha = \beta = 90°$, $\gamma = 120°$, V = 91.710 $Å^3$, Z=2

Atom	**Wyckoff sites**	**x**	**y**	**z**	**Occupancy**
K1	6h	0.6622	0.3311	0.2500	0.150
K2	2b	0.0000	0.0000	0.2500	0.239
Mn	2a	0.0000	0.0000	0.0000	0.947
O	4f	0.3333	0.6667	0.1057	1.000

Reliability index: Rwp = 5.98%, Rp = 4.17%.

Table S2. Structural parameters and atomic position of NMO from the Rietveld refinement.

Crystal System: hexagonal**, Space Group:** P63/mmc					
a = b = 2.8797 Å, c = 11.2273 Å, $\alpha = \beta = 90°$, $\gamma = 120°$, V = 80.632 Å^3, Z=2					
Atom	**Wyckoff sites**	**x**	**y**	**z**	**Occupancy**
Na1	2c	0.3333	0.6667	0.2500	0.362
Na2	2b	0.0000	0.0000	0.2500	0.308
Mn	2a	0.0000	0.0000	0.5000	1.000
O	4f	0.6667	0.3333	0.0736	1.000
Reliability index: Rwp = 5.94%, Rp = 5.43%.					

Table S3. Comparison of electrochemical performance of $K_{0.69}MnO_2$ sample with reported manganese-based layered oxide cathodes in SIBs.

Sample	Phase	Voltage (V vs. Na/Na^+)	Discharge Capacity	Cycling performance	Reference
$K_{0.69}MO_2$	P2	1.8-4.3	167.9 mAh g^{-1} @20 mA g^{-1}	87.6% (100 cycles) 50 mA g^{-1}	This work
$Na_{0.7}MnO_2$	P2	2.0-4.5	163 mAh g^{-1} @40 mA g^{-1}	65% (50 cycles) @40 mA g^{-1}	4
$Na_{0.67}Mn_{0.95}Mo_{0.05}O_2$	P2	1.8-4.3	163.9 mAh g^{-1} @20 mA g^{-1}	84.7% (100 cycles) @50 mA g^{-1}	5
$Na_{0.7}Fe_{0.7}Mn_{0.3}O_2$	P2	1.5-4.3	130 mAh g^{-1} @13 mA g^{-1}	61.5% (20 cycles) @13 mA g^{-1}	6
$Na_{2/3}Fe_{2/3}Mn_{1/3}O_2$	P2	1.5-4.2	151 mAh g^{-1} @25 mA g^{-1}	81.3% (10 cycles) @25 mA g^{-1}	7
$Na_{0.75}Ca_{0.05}Li_{0.15}Fe_{0.2}Mn_{0.6}O_2$	P2	1.5-4.3	183.8 mAh g^{-1} @22 mA g^{-1}	76% (150 cycles) @220 mA g^{-1}	8
$Na_{0.67}Mn_{0.64}Co_{0.3}Al_{0.06}O_2$	P2 /P3	1.5-4.0	160 mAh g^{-1} @20 mA g^{-1}	81% (200 cycles) @1000 mA g^{-1}	9
$Na_{2/3}Zn_{1/4}Mn_{3/4}O_2$	P2	1.5-4.5	202.4 mAh g^{-1} @20 mA g^{-1}	67% (50cycles) @20 mA g^{-1}	10
$Na_{2/3}Mn_{0.72}Cu_{0.22}Mg_{0.06}O_2$	P2	2.0-4.5	108 mAh g^{-1} @17.4 mA g^{-1}	87.9% (100 cycles) @174 mA g^{-1}	11
$K_{0.4}Fe_{0.1}Mn_{0.8}Ti_{0.1}O_2$	P3	1.8-4.0	160 mAh g^{-1} @20 mA g^{-1}	84% (30 cycles) @20 mA g^{-1}	12
$NaNi_{0.5}Mn_{0.5}O_2$	O3	2.2-3.8	120 mAh g^{-1} @8 mA g^{-1}	75% (50 cycles) @48 mA g^{-1}	13
$NaFe_{0.5}Ni_{0.5}O_2$	layer/tunnel	2.6-3.8	125 mAh g^{-1} @30 mA g^{-1}	83.1% (300 cycles) @1000 mA g^{-1}	14
$Na_{0.65}Mn_{0.75}Ni_{0.25}O_2$	P3	1.5-4.0	164 mAh g^{-1} @10 mA g^{-1}	75% (100 cycles) @20 mA g^{-1}	15
CTAB-$Na_{0.6}MnO_2$	tunnel	2.0-4.0	144.1 mAh g^{-1} @10 mA g^{-1}	89.5% (70 cycles) @ 10 mA g^{-1}	16
$Na_{0.7}MnO_{2.05}$@PPy	P2	1.8-4.4	160.3 mAh g^{-1} @100 mA g^{-1}	88.6%(100 cycles) 100 mA g^{-1}	17
$Na_{0.62}Ca_{0.025}Ni_{0.28}Mg_{0.05}Mn_{0.67}O_2$	P2	2.2-4.35	~135 mAh g^{-1} @50 mA g^{-1}	83%(100 cycles) 50 mA g^{-1}	18
$Na_{0.67}Mn_{0.95}Sn_{0.05}O_2$	P'2	1.5-4.0	212.4 mAh g^{-1} @10 mA g^{-1}	71.6%(200 cycles) 50 mA g^{-1}	19
$Na_{2/3}Fe_{1/3}Mn_{0.57}Ti_{0.1}O_2$	P2	1.5-4.3	154 mAh g^{-1} @32 mA g^{-1}	76%(50 cycles) 32 mA g^{-1}	20

References

1 J. J. Van Benschoten, J. Y. Lewis, W. R. Heineman, D. A. Roston and P. T. Kissinger, *J. Chem. Educ.*, 1983, **60,** 772.

2 L. Wang, C. Wang, N. Zhang, F. Li, F. Cheng and J. Chen, *ACS Energy Lett.*, 2017, **2,** 256.

3 Z. Geng, Y. C. Chien, M. J. Lacey, T. Thiringer and D. Brandell, *Electrochim. Acta*, 2022, **404,** 139727.

4 D. Su, C. Wang, H. Ahn, G. Wang, *Chem. Eur. J.*, 2013, 19, 10884.

5 L. Zhang, C. Wang, Y. Liu, M. Ren, J. Du, A. Chen, F. Li, *Chem. Eng. J.*, 2021, 426, 130813.

6 Y. Zhou, X. Wu, W. Wu, K. Wang, *Ceram. Int.*, 2014, 40, 13679.

7 E. Gonzalo, M. H. Han, J. M. López del Amo, B. Acebedo, M. Casas-Cabanas, T. Rojo, *J. Mater. Chem. A*, 2014, 2, 18523.

8 Y. Wang, X. Zhao, J. Jin, Q. Shen, N. Zhang, X. Qu, Y. Liu, L. Jiao, *Energy Storage Mater.*, 2022, 47, 44.

9 N. Jiang, Q. Liu, J. Wang, W. Yang, W. Ma, L. Zhang, Z. Peng, Z. Zhang, *Small*, 2021, 17, 2007103.

10 Y. Wang, L. Wang, H. Zhu, J. Chu, Y. Fang, L. Wu, L, Huang, Y. Ren, C. J. Sun, Q. Liu, X. Ai, H. Yang, Y. Cao, *Adv. Funct. Mater.*, 2020, 30, 1910327.

11 P. F. Wang, Y. Xiao, N. Piao, Q. C. Wang, X. Ji, T. Jin, Y. J. Guo, S. Liu, T. Deng, C. Cui, L. Chen, Y. G. Guo, X. Q. Yang, C. Wang, *Nano Energy*, 2020, 69,104474.

12 X. Zhang, D. Yu, Z. Wei, N. Chen, G. Chen, Z. Shen, F. Du, *ACS Appl. Mater. Interfaces*, 2021, 13, 18897.

13 S. Komaba, N. Yabuuchi, T. Nakayama, A. Ogata, T. Ishikawa, I. Nakai, *Inorg. Chem.*, 2012, 51, 6211.

14 Y. Nanba, T. Iwao, B. M. d. Boisse, W. Zhao, E. Hosono, D. Asakura, H. Niwa, H. Kiuchi, J. Miyawaki, Y. Harada, M. Okubo, A. Yamada, *Chem. Mater.*, 2016, 28, 1058.

15 Y. Wang, X. Wang, X. Li, R. Yu, M. Chen, K. Tang and X. Zhang, *Chem. Eng. J.*, 2019, 360, 139.

16 J. Zhang, H. Yuan, Y. Huang, S. Kan, Y. Wu, M. Bu, Y. Liu, P. He, H. Liu, *Chem. Eng. J.*, 2021, 417, 128097.

17 D. Lu, Z. Yao, Y. Zhong, X. Xia, C. Gu, J. Wu, J. Tu, *ACS Appl. Mater. Interfaces*, 2019, 11, 15630.

18 Fu H, Wang Y P, Fan G, et al. Synergetic stability enhancement with magnesium and calcium ion substitution for Ni/Mn-based P2-type sodium-ion battery cathodes[J]. Chemical science, 2022, 13(3): 726-736.

19 S. Li, Y. Zhang, K. Lei, Q. Yang, Z. Liu, K. Jiang, F. Li, Q. Lu, D. Mikhailova and S. Zheng, *J. Mater. Chem. A*, 2022, **10,** 10391.

20 Yang T, Huang Y, Zhang J, et al. Insights into Ti doping for stabilizing the Na2/3Fe1/3Mn2/3O2 cathode in sodium ion battery[J]. Journal of Energy Chemistry, 2022, 73: 542-548.